This article has been accepted for publication in a future issue of this journal, but has not been fully edited. Content may change prior to final publication. Citation information: DOI 10.1109/JSTARS.2020.2966432, IEEE Journal of Selected Topics in Applied Earth Observations and Remote Sensing

Snow Property Controls on Modelled Ku-band Altimeter Estimates of First-Year Sea Ice Thickness: Case studies from the Canadian and Norwegian Arctic

Vishnu Nandan[1,2], Randall K. Scharien[1], Torsten Geldsetzer[2], Ron Kwok[3], John. J. Yackel[2], Mallik S. Mahmud[2], Anja Rösel[4], Rasmus Tonboe[5], Mats Granskog[4], Rosemary Willatt[6], Julienne Stroeve[2,6], Daiki Nomura[7] and Markus Frey[8]

Abstract— **Uncertainty in snow properties impacts the accuracy of Arctic sea ice thickness estimates from radar altimetry. On first-year sea ice (FYI), spatiotemporal variations in snow properties can cause the Ku-band main radar scattering horizon to appear above the snow/sea ice interface. This can increase the estimated sea ice freeboard by several centimeters, leading to FYI thickness overestimations. This study examines the expected changes in Ku-band main scattering horizon and its impact on FYI thickness estimates, with variations in snow temperature, salinity and density derived from 10 naturally occurring Arctic FYI Cases encompassing saline/non-saline, warm/cold, simple/complexly layered snow (4 cm to 45 cm) overlying FYI (48 cm to 170 cm). Using a semi-empirical modeling approach, snow properties from these Cases are used to derive layer-wise brine volume and dielectric constant estimates, to simulate the Ku-band main scattering horizon and delays in radar propagation speed. Differences between modeled and observed FYI thickness are calculated to assess sources of error. Under both cold and warm conditions, saline snow covers are shown to shift the main scattering horizon above from the snow/sea ice interface, causing thickness retrieval errors. Overestimates in FYI thicknesses of up to 65% are found for warm, saline snow overlaying thin sea ice. Our simulations exhibited a distinct shift in the main scattering horizon when the snow layer densities became greater than 440 kg/m^3, especially under warmer snow conditions. Our simulations suggest a mean Ku-band propagation delay for snow of 39%, which is higher than 25%, suggested in previous studies.**

Index Terms— **Radar altimetry, snow, sea ice**

1. INTRODUCTION AND BACKGROUND

RADAR altimeters such as the ERS-1/2 RA, ENVISAT RA-2, CryoSat-2 and Sentinel-3A/B operating at Ku-band frequencies have been and are used to estimate sea ice freeboard, the vertical distance between local sea level and the snow/ice interface of floating sea ice [1-7]. Different retracking algorithms are used to obtain sea ice freeboard [2], [3], [8], [9]. Sea ice freeboard measurements derived from these algorithms are used in post-processing to estimate sea ice thickness, based on the hydrostatic equilibrium equation, as a function of snow thickness, snow density, sea ice density and sea water density [5].

Accounting for snow thickness is critical for accurately estimating sea ice thickness using radar altimetry. Generally, it is assumed that Ku-band microwaves attain complete penetration through dry, cold and homogeneous snow, and returns predominantly originate from the snow/sea ice interface [1], [3], [10-12]. However, these studies acknowledge that the presence of highly dense compacted snow layers and/or ice lenses may cause a vertical upward shift in the radar main scattering horizon towards the air/snow interface owing to complex surface and volume scattering mechanisms occurring within the snow volume. This shift leads to a misrepresentation of the sea ice freeboard (Figure 4 in [3]) and inaccurate sea ice thickness estimates, with the choice of thresholds in retracker algorithm also a factor [4]. Furthermore, recent studies acknowledge the variable penetration of Ku-band radar into the

Vishnu Nandan is with the Department of Geography, University of Victoria, BC, Canada and also with the Centre for Earth Observation Science, University of Manitoba, MB, Canada (e-mail: vishnu@uvic.ca)
Randall Scharien is with the Department of Geography, University of Victoria, BC, Canada (email: randy@uvic.ca)
Torsten Geldsetzer, John J. Yackel and Mallik S. Mahmud are with the Department of Geography, University of Calgary, AB, Canada (e-mail: geldsetz@ucalgary.ca, yackel@ucalgary.ca, msmahmud@ucalgary.ca)
Ron Kwok is with JPL, Caltech, USA (e-mail: Ronald.Kwok@jpl.nasa.gov)
Anja Rösel is with German Aerospace Center (DLR), Oberpfaffenhofen, Germany (e-mail: anja.roesel@dlr.de)
Mats Granskog is with the Norwegian Polar Institute, Fram Centre, Tromsø, Norway (e-mail: mats.granskog@npolar.no)
Rasmus Tonboe is with the Danish Meteorological Institute, Copenhagen, Denmark (e-mail: rtt@dmi.dk)
Rosemary Willatt and Julienne Stroeve are with the Centre for Polar Observation and Modelling, University College London, UK (email: r.willatt@ucl.ac.uk, j.stroeve@ucl.ac.uk)
Daiki Nomura is with the Faculty of Fisheries Science, Hokkaido University, Sapporo, Japan (email: daiki.nomura@fish.hokudai.ac.jp)
Markus Frey is with the British Antarctic Survey, Cambridge, UK (email maey@bas.ac.uk)

This article has been accepted for publication in a future issue of this journal, but has not been fully edited. Content may change prior to final publication. Citation information: DOI 10.1109/JSTARS.2020.2966432, IEEE Journal of Selected Topics in Applied Earth Observations and Remote Sensing

snow cover owing to snow moisture [12] and sub-footprint and footprint-scale surface roughness variations [12-16].

The effect of snow salinity on Arctic first-year sea ice (FYI) on microwave propagation and scattering has been long recognized [17-20]. Recently, it has gained renewed attention in the context of radar altimetry [14], [21-29]. Upward brine-wicking into the snow cover from the sea ice surface produces brine-wetted snow during all phases of the snow evolution history following sea ice freeze-up until spring/summer snow melt [17-20], [30]. The presence of brine alters the snow geophysical, thermodynamic, dielectric and microwave scattering properties [18], [19], [30], [31]. Microwave scattering and attenuation has been shown to occur within the snow cover [27], [29], to an extent which undoubtedly impacts radar-derived FYI thickness estimates. Brine in snow can also be due to heavy snow loading on relatively thin sea ice, where a negative freeboard leads to sea ice surface flooding by sea water [21], [22]. This in turn results in the formation of a highly saline slush layer that can freeze to form snow-ice [32] and produces highly saline snow [33-35]. Sea ice flooding is dependent on whether the sea ice is permeable or there exist potential pathways such as cracks [32], [36]. In the Arctic, flooding is likely to occur frequently in the Atlantic sector, which experiences more precipitation and thicker snow on thinner sea ice [36], [37] compared to other regions.

With recent Arctic amplification of warming caused by highly variable atmospheric forcing [38], Arctic sea ice has been experiencing increasing atmospheric moisture transport [39], rain-on-snow [40], and melt/refreeze events [41], [42]. The annual Arctic snow-covered FYI thermodynamic regime has changed, with warmer and more-complexly-layered late winter snow [40], [42], [44]. Snow with dense and compacted wind slabs, ice lenses, and crusts, significantly affects the Ku-band signal velocity and scattering [3], [67]. Furthermore, regional variations in atmospheric and oceanic forcing mechanisms are leading to shifts in snow and sea ice regimes [36], [44]. Increased open water areas and younger, thinner sea ice regimes, with high-salinity surfaces such as in the Norwegian Arctic and Canadian Arctic Archipelago, are becoming more common [45], [46]. The rapid rates of regional changes in sea ice conditions in the Arctic, as well as the Antarctic region [47], necessitates consistent updates in retrieval methods based on validated data products.

Recent simulations by [23] allude to the possible impact of snow salinity on Antarctic FYI freeboard and thickness estimates for Ku-band at the CryoSat-2 frequency. In [27], snow property data from the Canadian Arctic Archipelago is used to estimate a vertical shift up to 7 cm in the main scattering horizon of Ku-band energy in saline snow on FYI, leading to an overestimation of simulated FYI thickness by as much as 25%. To reduce snow salinity induced errors, they proposed a snow salinity correction factor for FYI freeboard estimates, valid for snow thicknesses ranging between 4 cm and 40 cm. The impact of snow salinity on Antarctic FYI freeboard and thickness estimates for Ku-band CryoSat-2 frequency is shown in [23]. A vertical shift of up to 8 cm in the CryoSat-2 scattering horizon in the Weddell Sea in the Antarctic is suggested in the study by [23]. Recent studies focused on the Atlantic sector of the Central Arctic (~ 83°N 21°E), demonstrated the impact of thick snow and negative ice freeboard on highly saline snow-ice formation and snow volume scattering, leading to overestimations, by a factor of 2, in sea ice thickness retrievals from CryoSat-2 compared to in situ measurements [21-22]. More work is required to improve the impact of snow property variations on Ku-band altimeter-derived FYI freeboard estimates, in order to improve FYI thickness estimates.

In this study, a semi-empirical modeling approach is used to examine the influence of snow temperature, salinity and density on the Ku-band main scattering horizon and resultaned FYI freeboard and ice thickness estimates. It builds on previous research by investigating 10 case studies of FYI from the Canadian and Norwegian Arctic, chosen to encompass a large range of conditions. The following questions are addressed:

1) How do snow temperature, salinity and density impact the Ku-band radar scattering horizon and estimated FYI freeboard and thickness?
2) How does simulated FYI thickness compare to in situ drill-hole measurements, as well as airborne, and satellite derived estimates?
3) Which snow property contributes the greatest error in simulated Ku-band altimeter-derived FYI freeboard and thickness estimates?
4) What is the effect of Ku-band radar propagation speed through saline snow on FYI?

Snow and sea ice data from the 10 Cases are provided in Section 2. Methods for simulating the main radar scattering horizon and estimating FYI freeboard and thickness are given in Section 3. The modeled Ku-band main scattering horizons for the 10 Cases are presented in Section 4, along with quantified differences between the measured FYI thicknesses and Ku-band simulated FYI thicknesses. Section 4 also presents a detailed sensitivity analysis of the effect of snow density has on the main scattering horizon and estimated FYI thickness, as well as the impact of brine on Ku-band radar propagation delay. Concluding statements are presented in Section 5.

2. Snow And sea ice properties

2.1 Snow Cases

In this study, each Case contains vertical profiles of snow density (ρ_S), snow salinity (S_S) and snow temperature (t_S). Variables were sampled at fixed 2 cm vertical intervals in the Canadian Arctic (CA), and at discrete intervals (depending on variability in snow properties observed during sampling) in the Norwegian Arctic (NA). 10 Cases were chosen from six separate field campaigns, encompassing a wide range of snow properties on FYI (Figure 1). CA samples were taken during the

This article has been accepted for publication in a future issue of this journal, but has not been fully edited. Content may change prior to final publication. Citation information: DOI 10.1109/JSTARS.2020.2966432, IEEE Journal of Selected Topics in Applied Earth Observations and Remote Sensing

late-winter season (May) on undeformed landfast FYI between 1993 and 2015. NA samples were taken in March 2015 and May 2017 as part of the 2015 Norwegian young sea ICE (N-ICE) expedition [44] and the 2017 INTPART Arctic Field Cruise [21], both onboard the R/V Lance.

Snow temperature measurements were made using a Digi-Sense RTD thermometer probe in CA (resolution of 0.1°C and accuracy of ± 0.2 °C) [29], and Testo 110 NTC temperature sensor (accuracy of ± 0.2 °C) [43] in NA. Snow density from both CA and NA was sampled using a 66.35 cm^3 density cutter (dimension ~ 3.5 cm × 5.5 cm × 3.5 cm) and weighed on a precision scale (accuracy of ± 0.01 g). Snow salinities from the CA and NA campaigns were measured using a WTW Cond 330i (accuracy of ± 0.5%) [29], and WTW Cond315i (accuracy of ± 0.5%) [43] conductivity meter, respectively, in the laboratory after the snow density samples melted and reached room temperature. Drill-hole FYI thickness ($T_{FYI(M)}$) was measured coincident and just adjacent to snow pits where snow property measurements were collected.

The 10 Cases were grouped according to snow thickness (H_S), with thin (< 10 cm), medium (10 – 30 cm) and thick (> 30 cm) classes used, to provide structure to the analysis. Bulk snow temperature was further used to identify Cases as cold (C) (mean t_S ≤ -10°C) or warm (W) (mean t_S > -10°C). Resulting Cases names are either ‘C’ or ‘W’ followed by the H_S value. For example, Case W4 represents a warm 4 cm snow cover (Table 1).

Figure 1 is located here

Table 1 is located here

Snow physical properties are shown in Figures 2-4. All three thin snow cover cases were found to be completely saline (Fig 2(b)).

Figure 2 is located here

Medium snow thickness Cases W12 and W16 are highly saline in the bottom 6 cm (~ 11 ppt), and relatively fresh in the topmost 4 cm (≤ 1 ppt) (Figure 3(b)). Medium thickness Case C24 is fresh, except for the bottom 1 cm, and Case W24 is saline in the bottom 12 cm (Figure 3(b)). C24 was likely flushed of brine by rain-on-snow event-initiated snow melt. A basal ice layer may have also inhibited upward brine migration from the FYI surface into the snow cover [42].

Figure 3 is located here

Thick Case W32 is a complexly-layered warm snow cover exhibiting a brine-free top 20 cm and relatively low salinity in the bottom 12 cm (mean S_S = 3.1 ppt) (Figure 4(b)). Thick Cases C36 and W45 are partially saline, with high salinity observed in the bottom 7 cm of both Cases (Figure 4(b)). The highly saline slush/snow-ice layers observed in the bottommost layers were observed to be due to sea ice surface flooding. No direct measurements of snow-ice salinity and temperature were made.

Although the 10 Cases encompass a large range of snow conditions on FYI, they are also representative of snow properties within the six field campaigns (Table 2), and snow on Arctic FYI. Common CA snow profiles such as those in [18], [26] are represented, as well as situations such as: complexly-layered snow covers that have been subjected to rain-on-snow/melt-refreeze events, observed in sub-Arctic environments [41]; and thick snow on thin ice subject to sea water infiltration, observed in the NA [21]. While it was not practical to capture all combinations of snow thickness, temperature and salinity profiles, the Cases are selected to encompass the range of scattering mechanisms likely occurring from snow profiles, collected from any one of the six campaigns.

Table 2 is located here

Figure 4 is located here

2.2 Snow layer characterization

All cases, except for the two Hudson Bay cases (C24 and W32), have three distinct layers: 1) a top snow layer of fragmented precipitation particles [49]; 2) a wind slab middle layer with rounded grains; and 3) a depth hoar layer (near the snow/sea ice interface). Case C24 is low-density snow overlaying a thin ice layer adhered to the FYI (Figure 3c). Case W32 is complexly-layered with 10 cm of decomposing and fragmented precipitation particles at the top, a 2 cm ice crust, a 2 cm snow layer, an 8 cm thick warming/rain-event ice layer, a 10 cm wind slab, and a 10 cm depth hoar layer with dispersed polyaggregate crystals (Figure 4(c)).

2.3 Ground-based, airborne and satellite radar derived snow thickness, FYI freeboard and sea ice thickness estimates

Regional-scale snow thickness and FYI freeboard and thickness measurements collected during N-ICE2015 and the 2017 INTPART field campaigns were acquired from a variety of ground-based, airborne and satellite-based radar sensors. These measurements are used for comparison to Ku-band simulated FYI thickness estimates, based on the snow Cases from the NA used in this study. Ground-based measurements comprised snow thickness measurements using an automatic position-recording snowhydro magnaprobe (n=1046), FYI freeboard and thickness measurements from in situ drill holes, and derived estimates of total snow and FYI thickness from an Geonics EM31 electromagnetic device (n=7005; N-ICE2015). The ultra-wideband frequency modulated continuous waveform (FMCW) snow radar and the airborne topographic

This article has been accepted for publication in a future issue of this journal, but has not been fully edited. Content may change prior to final publication. Citation information: DOI 10.1109/JSTARS.2020.2966432, IEEE Journal of Selected Topics in Applied Earth Observations and Remote Sensing

mapper (ATM) laser altimeter [50] onboard the NASA's Operation IceBridge (OIB) aircraft, which surveyed the N-ICE2015 study site on 19th March 2015, provided regional-scale estimates of snow thickness (n=227) and FYI freeboards and thicknesses. For comparison to Ku-band simulated FYI thickness, we also use the CryoSat-2 L2i (baseline C) radar altimeter data monthly mean FYI freeboard and derived thickness product from March 2015, acquired over the surveyed N-ICE2015 sites. No airborne or satellite radar altimeter derived estimates of FYI freeboard and thickness are related to Cases from CA.

3. METHODS

3.1 Modeled main scattering horizon

The main scattering horizon (S_H) is modeled as the vertical distance from the air/snow interface to the depth within the snow/sea ice volume where a Ku-band altimeter center frequency of 13.575 GHz signal undergoes dominant surface scattering (assuming negligible volume scattering [3]), at near-nadir incidence angle [27]. This method utilizes the simulated normalized echo power P_T at each n^{th} snow layer to estimate the location of S_H, which is the snow layer with maximum P_T. We consider the layer with the maximum P_T to be located at the 50% threshold point of the first local maximum of the Ku-band reflected return waveform, following [3] and [51]. The simulated P_T is obtained by [27],

$$P_{T(n\geq 2)} = (1 - P_{n-1}) * [\prod_{k=2}^{n-1}\{T_k(\theta') * \prod(1 - \prod_{k=2}^{n-1} L_k(\theta'))\}] * R_n(\theta') \quad (1a)$$

while $P_1 = R_1(\theta)$ (1b)

where $T(\theta')$ and $R(\theta')$ are the Ku-band vertically-polarized power transmission and reflection coefficients, respectively [52], given by

$$T(\theta') = \left[\frac{-\cos\theta' + \left(\frac{\sqrt{\varepsilon_1^*}}{\sqrt{\varepsilon_2^*}}\right)\cos\theta'}{\cos\theta' + \left(\frac{\sqrt{\varepsilon_1^*}}{\sqrt{\varepsilon_2^*}}\right)\cos\theta'}\right]^2 \text{ and } R(\theta') = 1 - T(\theta') \quad (1c)$$

where ε_1^* is the complex dielectric constant of the air or snow layer immediately above the calculated layer, and ε_2^* is the complex dielectric constant of the calculated layer. $T(\theta')$ and $R(\theta')$ are calculated for the upper surface of each snow layer, given the refracted incidence angle θ' in the snow layer immediately above it. The Ku-band $T(\theta')$ and $R(\theta')$ coefficients are modeled as functions of dry or brine-wetted snow dielectric permittivity and loss, calculated using the dielectric mixture model developed by [30]. The dielectric mixture model requires an estimate of brine volume fraction in snow φ_{bs}, which is a function of snow salinity, temperature and density, following [17] and [53]. We use the corresponding in situ measured snow property data to derive layer-wise snow φ_{bs} and dielectrics. $L(\theta')$ in (1a) is the two-way loss factor [54] given by

$$L(\theta') = \exp\left(\frac{-2K_e\tau}{\cos\theta'}\right) \quad (1d)$$

where K_e is the extinction coefficient given by $K_e = 1/\delta_p^\theta$ ([54] and supplementary information in [27]), where δ_p^θ is the radar penetration depth and τ is the snow layer thickness. θ in (1b) represents the incidence angle at near-nadir, where the altimeter signal interacts with the air/snow interface. A detailed description of model formulation and parameterization is provided in [27] (see supplementary information). The difference between S_H and H_S is the estimated shift in the scattering horizon ∇, located above, at, or below the sea ice freeboard. This shift is termed the '*snow property correction factor*'. ∇ is different from the Δ_S used in [27], since ∇ accounts for vertical shift caused by snow temperature, density and salinity, whereas Δ_S accounts for snow salinity only.

3.2 Sea ice thickness and radar freeboard

Sea ice freeboard (F_I) is the vertical distance between local sea level and the snow/sea ice interface. In general, isostatic equilibrium is assumed, and F_I is converted into an estimate of sea ice thickness (T_{FYI}), using

$$T_{FYI} = F_I \frac{\rho_W}{\rho_W - \rho_I} + H_S \frac{\rho_S}{\rho_W - \rho_I} \quad (2)$$

In this study, the in situ measured bulk snow density (ρ_S) and H_S is used to estimate T_{FYI} for each of the 10 Cases. The density of FYI (ρ_I) and sea water (ρ_W) were assumed to be 916.7 kg/m^3 and 1024 kg/m^3, respectively [1], [3], [55], [56]. F_I can be measured either in situ or estimated from an altimeter (F_R; radar freeboard). However, F_R is primarily dependent on the location of S_H and may not necessarily be the same as the actual measured F_I.

For FYI, F_R is assumed to be at a height other than F_I, due primarily to ∇ and C_W, given by

$$F_R = F_I + \nabla - C_W \quad (3)$$

where C_W is a correction factor to compensate for the reduced propagation delay through the snow cover as a function of H_S [57, 58], given by $C_W = \left(\frac{C_0}{C_{snow}} - 1\right) * H_S$; where C_0 is the speed of electromagnetic waves in a vacuum (3 × 10^8 m/s), $C_{snow} = C_0/\sqrt{|\varepsilon|}$, where C_{snow} is the speed of electromagnetic waves in snow and ε is the complex dielectric constant of dry/brine-wetted snow calculated using the dielectric mixture model developed by [30]. For dry snow, C_{snow}= 2.4 × 10^8 m/s [60], hence C_W = 0.25H_S [57].

3.3 Analysis Structure

To address research question 1, the 10 Cases were used to simulate the location of S_H and ∇, using (1a) and (1b). Using (2), the expected F_I was calculated, using drill-hole measured $T_{FYI(M)}$ and in-situ measured H_S and bulk ρ_S (Table 1) for all 10 Cases. F_R was estimated using (3) and $T_{FYI(F_R)}$ was predicted using the isostatic equilibrium condition (2), using F_R, instead of F_I. The percentage error (E_{FYI} in %) between the

This article has been accepted for publication in a future issue of this journal, but has not been fully edited. Content may change prior to final publication. Citation information: DOI 10.1109/JSTARS.2020.2966432, IEEE Journal of Selected Topics in Applied Earth Observations and Remote Sensing

measured and predicted altimeter-estimated FYI thickness was calculated to answer research question 2, using

$$E_{FYI}(\%) = \frac{T_{FYI(F_R)} - T_{FYI(M)}}{T_{FYI(M)}} \times 100 \quad (4)$$

Additionally, for Cases C36 and C45, we calculated the difference between $T_{FYI(M)}$ and FYI thicknesses derived from drill-hole, OIB and CryoSat-2 measurements from the N-ICE2015 and 2017 INTPART campaign surveyed ice floes. The above-mentioned steps together address research questions 1-3. For research question 3, we used a spectrum of snow layer ρ_S between 300 kg/m^3 and 500 kg/m^3 at 20 kg/m^3 steps, and recalculated F_R, $T_{FYI(F_R)}$ and E_{FYI}.

To address research question 4, we calculated C_{snow} and C_W for all Cases following [60], and compared C_{snow} obtained from all Cases to the same for the sample dry snow cover case used by [60]. To examine the validity of C_W = 0.25H_S for our Cases, we recalculated C_W at S_H with $C_{snow(S_H)} = C_0 / \sqrt{|\varepsilon_{S_H}|}$, where ε is the bulk complex dielectric constant of the snow volume between the snow surface and S_H.

4. RESULTS AND DISCUSSION

4.1 Local-scale snow and FYI thickness conditions in comparison to regional observations

The mean sea ice thickness of FYI dominated ice floes surveyed during N-ICE2015 was 95 cm, with snow thickness was 51 ± 0.07 cm (obtained from Figure 6 and Table 1 in [21]). Moreover, ~ 37% of the total area of the surveyed FYI floes were found to have negative freeboards, by up to 7 cm, similar to the Cases C36 and W45, used in this study. During the 2017 INTPART campaign, the mean snow and FYI thickness measurements were 41±23 cm and 165±50 cm, respectively (Table 3 in [21]). These observations suggest that the local-scale snow and FYI Cases from the NA used in our study are spatially and statistically representative of the overall regional-scale conditions. Additionally, these ranges fall within the range of snow thickness and FYI freeboard and thickness observations sampled through direct measurements from the N-ICE and INTPART campaigns.

4.2 Calculated FYI freeboards

FYI thickness ranged from 48 cm to 170 cm and thus encompassed the thin-, medium- and thick-FYI stages of development [48]. All cases except C36 and W45 produced positive F_I, derived from $T_{FYI(M)}$, with F_I ranging between 1.1 cm and 14.1 cm (Figure 5). Cases C36 and W45 from the NA were found to induce negative F_I of -4 cm and -6.6 cm, respectively, as expected given the large H_S relative to $T_{FYI(M)}$. Although snow-ice formation is expected with negative freeboards, we do not have snow-ice property measurements to incorporate into the radar scattering horizon model, so we use the observed snow property data only. This does not alter our goal to understand the relative errors that variable snow properties induce on $T_{FYI(F_R)}$.

Figure 5 is located here

4.3 Ku-band scattering horizon, FYI thickness retrieval and error analysis

4.3.1 Thin snow

Modeled layer-wise brine volume distribution and simulated Ku-band normalized echo power for thin snow cases are shown in Figure 6.

Figure 6 is located here

All thin snow cases illustrate how t_S can significantly impact Ku-band derived FYI thickness estimates, especially from brine-wetted snow on FYI. Despite much higher salinity for the cold case, strong differences in t_S result in similar φ_{bs} in the upper layers (φ_{bs}= 1% and 3%, for C4 and W6, respectively) that increase towards the snow/sea ice interface (φ_{bs}= 11% and 21%, for C4 and W6, respectively) (Figure 6(a)). This similarity in φ_{bs} results in a 1 cm ∇ difference, 3 cm for W4 and C6, and 4 cm for W6, respectively (Figure 6(b) and 9(b)). The cold case C6 and the warm cases W4 and W6 were associated with different $T_{FYI(M)}$, 130 cm compared to 100 cm and 48 cm, respectively, resulting in a substantially greater E_{FYI} for W6 (~51%), compared to ~19% (W4) and 11% (C6) (Figure 9(a)).

4.3.2 Medium snow

Modeled layer-wise φ_{bs} distribution and simulated normalized echo power for medium snow cases are shown in Figure 7. Cases W12 and W16 have similar bulk t_S but exhibit bulk S_S differences, ~ 4 ppt and ~ 8 ppt, respectively (Figure 3(b)). The ∇ for W12 is 4 cm and φ_{bs} is 0.7%, while the ∇ for W16 is 14 cm and φ_{bs} is 1.5%. The larger $T_{FYI(M)}$ of 170 cm combined with smaller ∇ for Case W12 results in a smaller E_{FYI} of 28%. For Case W16, smaller $T_{FYI(M)}$ of 130 cm combined with larger ∇ results in a greater E_{FYI} of 59% (Figure 9(a)). Case C24 is cold and mostly brine-free, scattering is at the snow/sea ice interface, and ∇ is zero. However, C_W of 6 cm, leads to an underestimated F_R of 4.2 cm (Equation 3), resulting in a negative E_{FYI} of 37% (i.e. $T_{FYI(F_R)} < T_{FYI(M)}$). This is an ideal example of a snow cover showcasing the utility of incorporating C_W added with F_R to obtain F_I. Case W24 is warm and saline, there is a ∇ of 13 cm and φ_{bs} ~ 0.85%, and E_{FYI} is 65% (Figure (7(a) and 9(a)).

Figure 7 is located here
Figure 8 is located here

4.3.3 Thick snow

Figure 8 shows modeled layer-wise φ_{bs} distribution and simulated normalized echo power for thick snow cases. Case W32 has relatively low φ_{bs} in its upper layers (φ_{bs} << 1%), with more in the basal snow layers (φ_{bs} ~ 3%) (Figure 8(a)).

This article has been accepted for publication in a future issue of this journal, but has not been fully edited. Content may change prior to final publication. Citation information: DOI 10.1109/JSTARS.2020.2966432, IEEE Journal of Selected Topics in Applied Earth Observations and Remote Sensing

Ku-band penetration is large and ∇ is 7 cm (Figure 9(b)). Of note is the effect of the 8 cm of highly dense ice layers within the snow volume (ρ_S of 877 kg/m^3). This layer causes a two-fold difference in dielectric permittivity between the snow layers (~ 1.6) and dense ice layers (~3.4). This layer produces a minor but early peak return accounting for ~15% of P_T (Figure 8(b)). Such layers, likely caused by a rain-on-snow event, have the potential to cause even greater F_R errors, (whereby ∇ can be falsely detected at 18 cm for Case W32; Figure 8(b)). Also notable is the effective compensation of ∇ for Case W32, negating the additive influence of F_R and C_W to obtain F_I which results in $T_{FYI(F_R)} \sim T_{FYI(M)}$.

Figure 9 is located here

Cases C36 and W45 exhibit negative freeboards with potential for saline slush and snow-ice formation. For modeling simplicity, we assume that the sea water infiltrated the basal snow layers and is frozen for both Cases. These basal snow layers turn into snow-ice and this effectively becomes the top of the sea ice, modifying the original negative freeboards from F_I = -4 cm and -6.6 cm to F_I = 0, for both Cases. The ∇ is 5 cm and 7 cm, due to wicking of sea water for C36 and W45, respectively (Figure 8(b) and 9(b)). Given the zero ice freeboards, F_R is -3 cm and -2.6 cm (Figure 9(b)). This, in addition to radar propagation delay (described in section 4.4), leads to negative F_R for both Cases. Given that negative F_R will generally cause an underestimation of sea ice thickness, for Case W45, the application of ∇ significantly dampens the error (i.e. $T_{FYI(F_R)} \sim T_{FYI(M)}$) (Figure 9(a)). On the other hand, for Case C36, the application of ∇ does not provide moderation to $T_{FYI(F_R)}$ estimates, resulting in an ~66% underestimation of sea ice thickness. Despite similar F_R for both Cases, the thinner and relatively less dense (bulk ρ_S = 175 kg/m^3) Case C36 likely resulted in this significant overestimation in $T_{FYI(F_R)}$, when compared to the relatively thicker and highly dense (bulk ρ_S = 351 kg/m^3) Case W45; however, this requires additional investigation. Recent observation-based analyses conducted by [21] and [22] in the NA reported similar findings with underestimation of CryoSat-2 measured sea ice thickness caused by negative freeboards. Moreover, their study used the modified Warren's snow climatology [55], [65] for snow thickness and snow density estimates to calculate sea ice thickness, which will also impact the accuracy of sea ice thickness retrievals. Their results, combined with those presented here, point to the need for detailed in situ measurements of snow, slush and snow-ice properties and modification in the scattering horizon model. This would enable quantitative examination of the impact of negative freeboard on Ku-band altimeter retracker algorithms and derived FYI thickness.

4.3.4 Comparing simulated FYI thickness with drill-hole, OIB and CryoSat-2 data

The FMCW snow radar onboard NASA's OIB airborne flight of the N-ICE2015 FYI floe yielded a mean snow thickness of 42±16 cm, which is underestimated relative to the magnaprobe derived snow thickness estimates of 58±15 cm (Table 3), though it is almost within the uncertainties. Coincident measured snow properties from snow pits analyzed during the airborne survey indicate basal layer snow salinity of up to 10 ppt (spatially representative of the C36 and W45 Cases). Moreover, one-third of the surveyed ice floe area was found to be flooded with substantial negative freeboards producing saline and saturated slush and snow-ice layers in the bottom of the snow pack. The mean FYI thickness, derived from the combination of snow radar and ATM was found to be 293 cm, which is overestimated by 95% relative to the Magnaprobe derived FYI thickness of 150 cm (Table 3). At the same time, the March 2015 monthly mean sea ice thickness from CryoSat-2 (using modified Warren's snow climatology from [55], [65]) over the N-ICE2015 surveyed ice floes is 220 cm, indicating a 47% overestimate, compared to $T_{FYI(M)}$ for Cases C36 and W45; this is consistent with our simulations. The overestimation in both CryoSat-2 and OIB snow radar derived FYI thicknesses is most likely triggered by the vertical shift in the main radar scattering horizon, caused by saline basal snow layers (through upward brine wicking) and underlying slushy layers (caused by sea water flooding) and a potentially slower Ku-band radar propagation speed.

Table 3 is located here

Among all of the Cases examined in this study, E_{FYI} are found to be highest for warm, saline snow covers overlying thin FYI, with E_{FYI} decreasing with increasing FYI thickness and for cold snow covers. However, it should be noted that saline snow covers are also very common under cold FYI conditions. Overall, the application of ∇ provides moderation to $T_{FYI(F_R)}$ estimates in addition to C_W, with largest impact on thicker snow covers overlying thicker FYI.

4.4 Sensitivity of Ku-band FYI thickness to snow density

Our study uses the bulk ρ_S measurements of each Case (Table 1) to estimate FYI freeboard and thickness at Ku-band frequency. However, the bulk ρ_S approach does not account for scattering effects caused by density inhomogeneities within a snow cover. These inhomogeneities modify the snow brine volume and the dielectrics between snow layers; likely impacting the location of the main scattering horizon. Therefore, to examine the sensitivity of inhomogeneous ρ_S on Ku-band altimeter derived FYI freeboard and thickness, we perform sensitivity analyses using a model 16 cm thick snow cover with a uniform S_S of 2 ppt, throughout the snow cover (at every 2 cm vertical intervals), overlying 150 cm thick FYI. This model snow pack is used to simulate the impact of ρ_S between 300 and 500 kg/m^3, iterated at 20 kg/m^3 steps, on ∇, $T_{FYI(F_R)}$ and E_{FYI}. Simulations representing cold (t_S = -15°C) and warm (t_S = -5°C) conditions were done (Figure 10). These results indicate that, at ρ_S between 340 kg/m^3 and 440 kg/m^3, ∇ is 1 cm and 3 cm for -15°C and -5°C, respectively; however, at 440 kg/m^3, ∇ increases to 5 cm at -15°C, and 11 cm at -5°C (Figure 10(a)).

Figure 10 is located here

This article has been accepted for publication in a future issue of this journal, but has not been fully edited. Content may change prior to final publication. Citation information: DOI 10.1109/JSTARS.2020.2966432, IEEE Journal of Selected Topics in Applied Earth Observations and Remote Sensing

At t_S = -5°C, ρ_S > 440 kg/m^3 and S_S = 2 ppt, we found substantial increase in the snow dielectric permittivity and dielectric loss by ~ 25%, that yielded an increase in ∇ (Figure 10(a)). Consequently, a significant overestimation in $T_{FYI(F_R)}$ by ~ 70% at ρ_S > 440 kg/m^3 and t_S = -5°C occurred (Figure 10(b,c)). At lower t_S = -15°C, the error is less, at 30%. Overestimation of ice thickness was found to be 20% lower when $\rho_S \leq$ 440 kg/m^3 and t_S = -5°C (Figure 10(c)).

It is evident based on these sensitivity analyses that snow density, when assessed in association with temperature and salinity, affects the accuracy of FYI freeboard and thickness retrieval from radar altimetry, and further points to the need for detailed analyses of its contribution to retrieval errors. Additionally, snow packs undergoing densification due to melt/refreeze/compaction and/or rain-on-snow events (for e.g. [67]), will likely add inhomogeneity, similar to Case W32 and will further confound the thickness retrieval estimate.

4.5 Ku-band propagation delay for brine-wetted snow covers

The delay in Ku-band radar propagation travelling through snow results in range retrieval errors and leads to sea ice thickness estimation errors. This has been previously observed in OIB [1], [55], [62], [63] and CryoSat-2 [3], [4], [60] studies. Saline snow layers also affect Ku-band signal propagation delay; however, this has not been previously considered. Our model currently does not account for layer-wise propagation delay in complexly-layered or brine-wetted snow as a function of snow thickness and brine volume; this warrants further research. Developing a propagation delay correction factor as a function of snow thickness (delay increases with thicker snow covers) and brine volume will help improve the accuracy of Ku-band altimeter derived FYI freeboard and thickness estimates, especially for snow exhibiting a wide range of geophysical and thermodynamic properties. Nevertheless, as a first estimate of the impact of salinity on Ku-band signal propagation delay, the bulk complex dielectric constant (ε) from all 10 Cases was used to derive a propagation speed C_{snow} following [59] (Figure 11). This is compared to $C_{snow(dry)}$ = 2.428 × 10^8 m/s used by [60] for dry snow. There is a 51% mean reduction in Ku-band propagation speed for saline snow covers using C_{snow} instead of $C_{snow(dry)}$ (Figure 11). As expected, the largest relative reductions (up to 70%) in propagation speed are observed for warm, saline snow covers cases, whereas, for example, the C24 relatively cold and non-saline snow cover does not exhibit any relative reduction in speed. Delays in Ku-band propagation speed may significantly affect the accuracy of FYI freeboard and thickness estimates and warrants further investigation.

Figure 11 is located here

We also evaluated the robustness of using the 25% radar propagation delay proposed by [57], for snow covers exhibiting a vertical shift in the main scattering horizon, as a function of S_H. To quantify the variability in the propagation delay as a function of brine wetting still present in the snow layers above S_H, we calculated $C_{snow(S_H)}$ for all Cases separately, and derived its mean, to provide a first estimate of C_W for such situations. Figure 11 shows considerable variability in $C_{snow(S_H)}$ with a mean reduction of 39% in the radar propagation speed for all Cases, including the low-salinity layers lying above S_H. When the whole snow volume, including the saline snow layers, are considered, a mean reduction of 51% was observed for all Cases. Also to be noted is the 25% delay factor, if the snow layers lying above S_H were non-saline. The higher delay factor derived from this study holds true for the wide range of snow Cases used in this study, although further research is warranted to investigate and validate our findings to broader spatial footprints.

4.6 Main scattering horizon model validity and limitations

The main scattering horizon model used in this study is valid for smooth, snow-covered FYI assumed to be homogenous within an altimeter footprint. A fully realized scattering model would need to account for surface and interface roughness effects, as well as additional scattering contributions to the total radar echo not represented by Rayleigh scattering and first-order surface scattering effects. This latter limitation is especially true at higher frequencies such as Ku- and Ka-bands. On the other hand, a model intended for representation of altimeter footprints would have to account for inhomogenous surfaces [64].

The model is invalid when the snow is dominated by larger grains and/or where there is more than one snow grain scatterer (spherical) with dimension(s) of the order of the Ku-band wavelength. In such instances, the model needs to include Mie scattering contributions [52]. This situation results in significant volume scattering within the snow pack [25], which the model used in this study currently does not consider. It should be noted that currently operational retracking algorithms also assume the volume scattering to be negligible. Nevertheless, the model would benefit from parameterizing snow grain size with proven and reliable methods, to include a volume scattering component. The model also requires additional parameterization in the event of slush and snow-ice formation, as the radar propagation response will be likely different. Moreover, a snow thickness and brine volume-dependent correction factor needs to be developed and incorporated into the main scattering horizon model, accounting for changes in atmospheric forcing history (such as diurnal variability in meteorological conditions during late-winter season, prior to melt-onset) and Ku-band radar propagation delay.

5. Conclusions and Future Work

This study has outlined the expected changes in Ku-band radar main scattering horizon with variable snow properties observed from 10 naturally occurring Arctic FYI Cases encompassing saline/non-saline, warm/cold, simple/complexly layered, thin, medium and thick snow (4 cm to 45 cm) overlying thin, medium and thick FYI (48 cm to 170 cm). Snow and ice properties are sampled at locations in the Canadian and the Norwegian Arctic, during late-winter (March to May) seasons

This article has been accepted for publication in a future issue of this journal, but has not been fully edited. Content may change prior to final publication. Citation information: DOI 10.1109/JSTARS.2020.2966432, IEEE Journal of Selected Topics in Applied Earth Observations and Remote Sensing

between 1993 and 2017. The impact on Ku-band altimeter derived FYI freeboard and thickness estimates is also assessed. A semi-empirical modeling approach to evaluate differences between Ku-band simulated and in situ drill-hole measured FYI thickness is presented and validated using remotely sensed FYI thickness retrievals from the Norwegian Arctic. The case studies represent past, current, as well as likely future late-winter Arctic FYI conditions, especially in the Canadian and Norwegian Arctic, and illustrate potential impacts on Ku-band radar altimeter derived FYI freeboard and thickness estimates, assuming surface homogeneity within the altimeter footprint. We addressed the following four questions.

1) ***How do snow temperature, salinity and density impact the Ku-band radar scattering horizon and estimated FYI freeboard and thickness?***

Irrespective of location, high snow salinity and warm snow temperature leads to higher brine volume and greater dielectric loss. This induces significant Ku-band microwave absorption within the snow pack, vertically shifts the Ku-band main scattering horizon, and subsequently prevents the Ku-band signal from reaching the snow/sea ice interface. We present a '*snow property correction factor*' ∇, which quantifies the vertical shift and dampens the error in Ku-band simulated sea ice freeboard and thickness estimates. For warm and saline snow Cases, simulated radar freeboard is greater than actual sea ice freeboard, leading to overestimated FYI thickness, compared to drill-hole measurements. The vertical shift in the scattering horizon with corresponding discrepancies is also observed in OIB snow radar- and CryoSat-2 derived FYI freeboard and thickness retrievals from the Norwegian Arctic. This phenomenon is presently characteristic to snow-covered FYI, in the Canadian and Norwegian Arctic. FYI near large river outflows or in low-salinity brackish waters, such as the Gulf of Bothnia, and MYI types will likely not exhibit this effect due to freshening at the surface; however, this warrants further investigation.

2) ***How does simulated FYI thickness compare to in situ drill-hole measurements, as well as airborne, and satellite derived estimates?***

Differences between in situ drill-hole measured FYI thickness and Ku-band simulated thicknesses were observed for Cases where a vertical shift in the radar scattering horizon occured. The highest FYI thickness retrieval errors, up to 65%, are associated with warm, highly saline snow overlying thin ice. As expected, based on previous work on the Canadian Arctic Archipelago [27], retrieval errors were found to decrease with an increase in FYI thickness and when snow is cold and relatively non-saline (for example, Case C24). In the Norwegian Arctic, especially for Cases C36 and W45 which were spatially representative of snow covers measured from NASA's Operation IceBridge and CryoSat-2, our study found >100% overestimation in estimated FYI thickness compared to in situ drill hole measurements. This overestimation is attributed to saline basal snow layers, caused by upward brine wicking from sea ice surface and saline slushy and snow-ice layers produced by sea water flooding caused by thicker snow loading. As such, Ku-band microwaves are largely prevented from reaching the snow/sea ice interface.

3) ***Which snow property contributes the greatest error in simulated Ku-band altimeter-derived FYI freeboard and thickness estimates?***

The salinity of both warm and cold snow was found to be the dominant snow property affecting the accuracy of Ku-band altimeter derived FYI freeboard and thickness estimates. As demonstrated, the radar scattering horizon is also sensitive to variations in snow density. For snow layer densities between 300 kg/m^3 and 500 kg/m^3, the radar scattering horizon is mostly impacted by snow layer densities greater than 440 kg/m^3, specifically when the snow is warm. Also of note is the possible impact of snow density and snow thickness on ice thickness estimates for snow covers exhibiting similar radar freeboard (observed for Cases C36 and W45). However, further research is needed to evaluate this scenario and to to investigate the impact of inhomogeneous snow layers caused by melt-refreeze and rain-on-snow events towards accurately locating the main radar scattering horizon.

4) ***What is the effect of Ku-band radar propagation speed through saline snow on FYI?***

Ku-band radar propagation delay is affected by the presence of saline snow and vertically shifting radar scattering horizon. Compared to current operational retracker algorithms, which use a 25% propagation delay factor, a 39% delay in radar propagation is estimated here from the mean of 10 snow Cases. From a sea ice monitoring perspective, this modeling study suggests a higher factor should be considered for certain conditions, however, this awaits further validation through coordinated satellite and field observations from field campaigns such as during the 2019-2020 Multidisciplinary drifting Observatory for the Study of Arctic Climate (MOSAiC) (https://www.mosaic-expedition.org/about-mosaic/the-science.html).

Our study reveals underestimation in simulated FYI thickness retrievals for cases exhibiting negative ice freeboards. This phenomenon is now commonly observed in the Norwegian Arctic [21], [22] and is associated with slush/snow-ice formation [32], [36], resulting in additional snow property variability. Results indicate that additional slush/snow-ice property data needs to be collected in order to semi-empirically model this scenario in detail.

Considering the large variability in snow and sea ice geophysical conditions observed in our study, future research should conduct similar analyses based on a comprehensive dataset of seasonally and regionally representative snow measurements, to identify the expected snow salinity impact on Ku-band sea ice thickness retrievals for the Arctic and its sub-regions. Additionally, detailed investigation should also be conducted using snow/sea ice geophysical properties collected (for e.g. MOSAiC) during the early-winter season (December to March period), and also to investigate changes in the radar scattering horizon, as a function of atmospheric forcing history. This is critical, especially during the late-winter season, when diurnal oscillations in air temperature and changes in precipitation patterns (both leading to melt/refreeze events), will likely affect Ku-band radar propagation through snow covers on FYI.

Future research should also focus on refining currently existing altimeter backscatter models (e.g. [16]) and operational retracker algorithms, by accounting for: 1) potential Ku-band volume scattering from larger snow grains and snow as a dense media (e.g. transition from Rayleigh to Mie scattering); 2) inhomogeneous footprints especially across marginal ice zones and multi-year ice surfaces with refrozen melt ponds and hummocks; 3) geophysical complexities introduced by slush and snow-ice formation, induced by negative freeboards; and 4) radar propagation delay in complexly layered or brine-wetted snow covers. Our forthcoming research will focus on validating the modeling framework and theoretical findings from this study through current field campaigns such as the MOSAiC, using in situ snow/sea ice property data combined with coincident surface-based, airborne and satellite borne multi-frequency scatterometer and radar altimeter data towards improved estimates of Arctic FYI thickness measurements..

List of Symbols Frequently Used in the Study

Symbols	Description (Unit)
ρ_S	Snow density (kg/m^3)
S_S	Snow salinity (ppt)
t_S	Snow temperature (°C)
φ_{bs}	Snow brine volume (%)
H_S	Snow thickness (cm)
S_H	Ku-band main scattering horizon (cm)
P_T	Ku-band simulated normalized echo power
∇	Snow property correction factor (cm)
F_R	Radar-derived FYI freeboard (cm)
F_I	FYI freeboard (cm)
C_W	Radar propagation delay (cm)
$T_{FYI(M)}$	Drill-hole measured FYI thickness (cm)
$T_{FYI(F_R)}$	Ku-band simulated FYI thickness (cm)
E_{FYI}	Percentage error (%)

Data and Algorithm Availability Statement

The snow/sea ice geophysical property data from the Canadian Arctic used in this study are available upon request, from the corresponding author. The N-ICE2015 snow/sea ice geophysical property data and remote sensing datasets are publicly available via https://data.npolar.no/dataset/?filter-links.rel=data&q=n-ice2015. The snow/sea ice geophysical property data from the 2017 INTPART campaign are available upon request, from the corresponding author. The algorithm used in this study will be publicly available soon through IEEE's Remote Sensing Code Library via https://rscl-grss.org/index.php.

Acknowledgements

The authors thank Mark Christopher Fuller (University of Manitoba) for assistance with snow and sea ice thickness and geophysical property data collection; Natural Sciences and Engineering Research Council of Canada (NSERC) Discovery and Polar Knowledge Canada (POLAR) (#NST-1718-0024) grants to Randall Scharien and John Yackel; Marine Environmental Observation, Prediction and Response Network (MEOPAR) Postdoctoral Fellowship grant to Vishnu Nandan; Natural Environment Research Council (NERC) UK (NE/M005852/1) to Markus Frey. The authors also thank the crew of R/V Lance and all members of the N-ICE2015 expedition for their support in conducting the field work. This expedition was supported by Research Council of Norway (KLIMAFORSK programme, #240639), the Centre of Ice, Climate and Ecosystems (ICE) at the Norwegian Polar Institute through the N-ICE project, the Ministry of Climate and Environment and the Ministry of Foreign Affairs of Norway, the Grant for Joint Research Program of the Institute of Low Temperature Science, Hokkaido University, the Grant for Arctic Challenge for Sustainability, and the Japan Society for the Promotion of Science (#15K16135, #24-4175). David Barber at the Centre for Earth Observation Science, University of Manitoba is acknowledged for financial and logistical support for collection of field data.

References

[1] S. Laxon, k. A. Giles, A. L. Ridout, D. J. Wingham, R. Willatt, R. Cullen, R. Kwok, A. Schweiger, J. Zhang, C. Haas, S. Hendricks, R. Krishfield, N. Kurtz, S. Farrell and M. Davidson, "CryoSat-2 estimates of Arctic sea ice thickness and volume," *Geophys. Res. Lett*., vol. 40, no. 4, pp. 732-737, Feb. 2013.

[2] N. T. Kurtz, N. Galin and M. Studinger, "An improved CryoSat-2 sea ice freeboard retrieval algorithm through the use of waveform fitting," *The Cryosphere*., vol. 8, no. 4, pp. 1217-1237, July. 2014.

[3] R. Ricker, S. Hendricks, V. Helm, H. Skoroup and M. Davidson, "Sensitivity of CryoSat-2 Arctic sea-ice freeboard and thickness on radar-waveform interpretation," *The Cryosphere*., vol. 8, no. 4, pp. 1607-1622, Aug. 2014.

[4] R. Ricker, S. Hendricks, V. Helm and R. Gerdes, "Impact of snow accumulation on CryoSat-2 range retrievals over Arctic sea ice: An observational approach with buoy data," *Geophys. Res. Lett*., vol. 42, no. 11, pp. 4447-4455, June. 2015.

[5] S. Laxon, N. Peacock and D. Smith, "High interannual variability of sea ice thickness in the Arctic region," *Nature*, vol. 425, no. 6961, pp. 1176-1193, Oct. 2003.

[6] R. Kwok and G. F. Cunningham, "Variability of Arctic sea ice thickness and volume from CryoSat-2," *Phil. Trans. R. Soc. A*, vol. 373, no. 2045, pp. 20140157, July. 2015.

[7] R. L. Tilling, A. Ridout and A. Shepherd, "Near-real-time Arctic sea ice thickness and volume from CryoSat-2," *The Cryosphere*., vol. 10, no. 5, pp. 2003-2012, Sep. 2016.

[8] X. Shen, M. Similä, W. Dierking, X. Zhang, C. Ke, M. Li and M. Wang, "A New Retracking Algorithm for Retrieving Sea Ice Freeboard from CryoSat-2 Radar Altimeter Data during Winter–Spring Transition," *Remote Sensing*, vol. 11, no. 10, pp. 1-20, May. 2019.

[9] R. L. Tilling, A. Ridout, A. Shepherd and D. J. Wingham, "Increased Arctic sea ice volume after anomalously low melting in 2013," *Nature Geoscience*, vol. 8, pp. 643-646, July. 2015.

[10] S. G. Beaven, G. L. Lockhart, S. P. Gogineni, A. R. Hosseinmostafa, K. Jezek, A. J. Gow, D. K. Perovich, A. K. Fung and S. Tjuatja. "Laboratory

measurements of radar backscatter from bare and snow-covered saline ice sheets," *Int. J. Remote Sens.*, vol. 16, no. 5, pp. 851-876, May. 1995.

[11] S. Hendricks, R. Ricker and V. Helm, "AWI CryoSat-2 Sea Ice Thickness Data Product (v1.2)," http://data.meereisportal.de/data/cryosat2/doc/AWI_CryoSat2_Documentation_current, July, 2016

[12] S. Hendricks, L. Stenseng, V. Helm and C. Haas, "Effects of surface roughness on sea ice freeboard retrieval with an Airborne Ku-Band SAR radar altimeter," *2010 IEEE Int. Geosci. and Remote Sens. Sympo.*, pp. 3126-3129, July. 2010.

[13] R. Kwok, "Simulated effects of a snow layer on retrieval of CryoSat-2 sea ice freeboard". *Geophys. Res. Lett.*, vol. 41, no. 14, pp. 5014-5020, July. 2014.

[14] R. Tonboe, S. Andersen and L. T. Pedersen, "Simulation of the Ku-band radar altimeter sea ice effective scattering surface," *IEEE Geosci. Remote Sens Letters*, vol. 3, no. 2, pp. 237-240, April. 2006.

[15] R. Tonboe, S. Andersen, R. S. Gill and L. T. Pedersen, "The simulated seasonal variability of the Ku-band radar altimeter effective scattering surface depth in sea ice", *Arctic Sea Ice Thickness: Past, Present and Future, in Climate Change and Natural Hazards Series*, vol. 10, EUR22416, July. 2006.

[16] R. Tonboe, L. T. Pedersen and C. Haas, "Simulation of the Cryosat-2 satellite radar altimeter sea ice thickness retrieval uncertainty," *The Cryosphere*, vol. 3, no. 1, pp. 513-559, July. 2009.

[17] M. R. Drinkwater and G. B. Crocker, "Modelling changes in the dielectric and scattering properties of young snow-covered sea ice at GHz frequencies," *J. of. Glaciolo*., vol. 34, no. 118, pp. 274-282. Feb. 1988.

[18] D. G. Barber and S. V. Nghiem, "The role of snow on the thermal dependence of microwave backscatter over sea ice," *J. Geophys. Res.*, vol. 104, no. C11, pp. 25789-25803, Nov. 1999.

[19] D. G. Barber, A. K. Fung, T. C. Grenfell, S. V. Nghiem, R. G. Onstott, V. L. Lytle, D. K. Perovich and A. J. Gow, "The Role of Snow on Microwave Emission and Scattering over First-Year Sea Ice," *IEEE Trans. Geosci. Remote Sens*., vol. 36, no. 5, pp. 1750-1763, Sep. 1998.

[20] K. C. Jezek, D. K. Perovich, K. M. Golden, C. Luther, D. G. Barber, P. Gogineni, T. C. Grenfell, A. K. Jordan, C. B. Mobley and S. V. Nghiem, "A broad spectral, interdisciplinary investigation of the electromagnetic properties of sea ice," *IEEE Trans. Geosci. Remote Sens*., vol. 36, no. 5, pp. 1633-1641, Sep. 1998.

[21] A. Rösel, P. Itkin, J. King, D. Divine, C. Wang, M. A. Granskog, T. Krumpen and S. Gerland, "Thin Sea Ice, Thick Snow, and Widespread Negative Freeboard Observed During N-ICE2015 North of Svalbard," *J. Geophys. Res.*, vol. 123, no. 2, pp. 1156-1176, Feb. 2018.

[22] J. King, H. Skoroup, S. M. Hvidegaard, A. Rösel, S. Gerland, G. Spreen, C. Polashenski, V. Helm and G. E. Liston, "Comparison of Freeboard Retrieval and Ice Thickness Calculation From ALS, ASIRAS, and CryoSat-2 in the Norwegian Arctic to Field Measurements Made During the N-ICE2015 Expedition," *J. Geophys. Res.*, vol. 123, no. 2, Feb. 2018.

[23] R. Kwok and S. Kacimi, "Three years of sea ice freeboard, snow depth, and ice thickness of the Weddell Sea from Operation IceBridge and CryoSat-2," *The Cryosphere*, vol. 12, pp. 2789-2801, Aug. 2018.

[24] I. R. Lawrence, M. C. Tsamados, J. C. Stroeve, T. W. K. Armitage and A. L. Ridout, "Estimating snow depth over Arctic sea ice from calibrated dual-frequency radar freeboards," *The Cryosphere*, vol.12, pp. 3551-3564, April. 2018.

[25] V. Nandan, T. Geldsetzer, T. Islam, J. J. Yackel, J. P. S. Gill and M. Mahmud, "Multifrequency Microwave Backscatter From a Highly Saline Snow Cover on Smooth First-Year Sea Ice: First-Order Theoretical Modeling," *IEEE Trans. Geosci. Remote Sens*., vol. 55, no. 4, pp. 2177-2190, April. 2017.

[26] V. Nandan, R. Scharien, T. Geldsetzer, M. Mahmud, J. J. Yackel, T. Islam, J. P. S. Gill, M. C. Fuller, G. Gunn and C. Duguay, "Geophysical and atmospheric controls on Ku-, X- and C-band backscatter evolution from a saline snow cover on first-year sea ice from late-winter to pre-early melt," *Remo. Sens. Environ.* vol. 198, pp. 425-441, Sep. 2017.

[27] V. Nandan, T. Geldsetzer, J. Yackel, M. Mahmud, R. Scharien, S. Howell, J. King, R. Ricker and B. Else. "Effect of Snow Salinity on CryoSat-2 Arctic First-Year Sea Ice Freeboard Measurements," *Geophys. Res. Lett*., vol. 44, no. 20, pp. 10419-10426, Oct. 2017.

[28] J. J. Yackel, J. P. S. Gill, T. Geldsetzer, M. C. Fuller and V. Nandan. "Diurnal Scale Controls on C-Band Microwave Backscatter From Snow-Covered First-Year Sea Ice During the Transition From Late Winter to Early Melt," *IEEE Trans. Geosci. Remote Sens*., vol. 55, no. 7, pp. 3860-3874, April. 2017.

[29] V. Nandan, T. Geldsetzer, T. Islam, J. J. Yackel, J. P. S. Gill, M. C. Fuller, G. Gunn and C. Duguay, "Ku-, X- and C-band measured and modeled microwave backscatter from a highly saline snow cover on first-year sea ice," *Remote. Sens. Env*, vol. 187, pp. 62-75, Dec. 2016.

[30] T. Geldsetzer, A. Langlois and J. J. Yackel, "Dielectric properties of brine wetted snow on first-year sea ice," *Cold Reg. Sci. and Tech.* vol. 58: no. 1-2, pp. 47–56, Aug. 2009.

[31] S. V. Nghiem, R. Kwok, S. Yueh and M. R. Drinkwater, "Polarimetric signatures of sea ice. Part 2: Experimental Observations," *J. Geophys. Res.*, vol. 100, no. C7, pp. 25789-25803, July. 1995.

[32] M. A. Granskog, A. Rösel, P. Dodd, D. Divine, S. Gerland, T. Martma and M. J. Leng, "Snow contribution to first-year and second-year Arctic sea ice mass balance north of Svalbard," *J. Geophys. Res.*, vol. 122, no. 3, pp. 2539-2549, March. 2017.

[33] M. Sturm and R. A. Massom, "Snow and sea ice," *Sea Ice. Oxford, Wiley-Blackwell*, pp. 153-204, Nov. 2010.

[34] C. Wang, B. Cheng, R. Graham, A. Rösel and M. A. Granskog, "Critical role of snow on sea ice growth in the Atlantic sector of the Arctic Ocean," *Geophys. Res. Lett*., vol. 44, no. 20, pp. 10479-10485, Oct. 2017.

[35] C. Haas, D. N. Thomas and J. Bareiss, "Surface properties and processes of perennial Antarctic sea ice in summer," *Journal Glac*, vol. 47, no. 159, pp. 613-625, Dec. 2001.

[36] I. Merkouriadi, J-C. Gallet, R. M. Graham, G. E. Liston, C. Polashenski, A. Rösel and S. Gerland, "Winter snow conditions on Arctic sea ice north of Svalbard during the Norwegian young sea ICE (N-ICE2015) expedition," *J. Geophys. Res.*,, vol. 122, no. 20, pp. 10837-10854, Oct. 2017.

[37] M. A. Webster, C. Parker, L. Boisvert, R. Kwok, "The role of cyclone activity in snow accumulation on Arctic sea ice," *Nat Commun*, Vol. 10, No. 5285, Nov 2019.

[38] J. A. Francis, S. J. Varvus and J. Cohen, "Amplified Arctic warming and mid-latitude weather: new perspectives on emerging connections," *Wiley Interdis. Reviews: Climate Change*, vol. 8, no. 5, pp. e474, Oct. 2017.

[39] J. Mortin, G. Svensson, R. G. Graversen, M. L. Kapsch, J. C. Stroeve and L. N. Biosvert, "Melt onset over Arctic sea ice controlled by atmospheric moisture transport," *Geophy. Resear. Lett*, vol. 43, no. 12, pp. 6636-6642, June. 2016.

[40] A. Langlois, C. A. Johnson, B. Montpetit, A. Royer, E. A. Blukacz-Richards, E. Neave, C. Dolant, A. Roy, G. Arhonditsis, D-K. Kim, S. Kaluskar and L. Brucker, "Detection of rain-on-snow (ROS) events and ice layer formation using passive microwave radiometry: A context for Peary caribou habitat in the Canadian Arctic," *Remote. Sens. Environ.*, vol. 189, pp. 84-95, Feb. 2017.

[41] M. C. Fuller, T. Geldsetzer, J. Yackel and J. P. S. Gill, "Comparison of a coupled snow thermodynamic and radiative transfer model with in situ active microwave signatures of snow-covered smooth first-year sea ice," *The Cryosphere*, vol. 9, pp. 2149-2161, Nov. 2015.

[42] M. C. Fuller, T. Geldsetzer, J. P. S. Gill, J. J. Yackel and C. Derksen, "C-band backscatter from a complexly-layered snow cover on first-year sea ice," *Hydro. Proc.*, vol. 28, no. 16, pp. 4614-4625, July. 2014.

[43] D. Nomura, M. A. Granskog, A. Fransson, M. Chierici, A. Silyakova, K. I. Ohshima, L. Cohen, B. Delille, S. R. Hudson, and G. S. Dieckmann, "CO_2 flux over young and snow-covered Arctic pack ice in winter and spring," *Biogeosciences*, vol. 15, pp. 3331-3343, June. 2018.

[44] J-C. Gallet, I. Merkouriadi, G. E. Liston, C. Polashenski, S. Hudson, A. Rösel and S. Gerland, "Spring snow conditions on Arctic sea ice north of Svalbard, during the Norwegian Young Sea ICE (N-ICE2015) expedition," *J. Geophys. Res.*, vol. 122, pp. 10820-10836, Oct. 2017.

[45] V. S. Lien, P. Schlichtholz, Ø. Skagseth and F. B. Vikebø, "Wind-Driven Atlantic Water Flow as a Direct Mode for Reduced Barents Sea Ice Cover," *Journal of Climate*, vol. 30, no. 2, pp. 803-812, Jan. 2017.

[46] J. E Box, W. T Colgan, T. R. Christensen, N. M. Schmidt, M. Lund, F-J. W. Parmentier, R. Brown, U. S. Bhatt, E. S. Euskirchen, V. E. Romanovsky, J. E. Walsh, J. E. Overland, M. Wang, R. W. Corell, W. N. Meier, B. Wouters, S. Mernild, J. Mård, J. Pawlak and M. S. Olsen, "Key indicators of Arctic climate change: 1971–2017," *Env. Research Letters*, vol. 14, no. 4, pp. 045010, April. 2019.

[47] J. Turner, J. S. Hosking, G. J. Marshall, T. Phillips and T. J. Bracegirdle, "Antarctic sea ice increase consistent with intrinsic variability of the Amundsen Sea Low," *Climate Dynamics*, vol. 47, no. 7, pp. 2391-2402, April. 2016.

[48] WMO, "World Meteorological Organization: sea-ice nomenclature," *Sea-ice Nomencl. WMO/OMM/BMO - No.259 Ed. 1970 – 2004*, no. 259, pp. 147, May. 1970.

[49] C. Fierz, R. L. Armstrong, Y. Durand, P. Etchevers, E. Greene, D. M. McClung, K. Nishimura, P. K. Satyawali and S. A. Sokratov, "The International classification for seasonal snow on the ground," *International Association of Cryospheric Sciences*, SC.2009/WS/15, 90p, April. 2009.

[50] T. Newman, S. L. Farrell, J. Richter-Menge, L. N. Connor, N. T. Kurtz, B. C. Elder and D. McAdoo, "Assessment of radar-derived snow depth over Arctic sea ice," *J. Geophys. Res.*, vol. 119, no. 12, pp. 8578-8602, Dec. 2014.

[51] C. H. Davis, "A robust threshold re-tracking algorithm for measuring ice-sheet surface elevation change from satellite radar altimeters," *IEEE Trans. Geosci. Remote Sens*., vol. 35, no. 4, pp. 974-979, July. 1997.

[52] P. Lorrain, D.R. Corson and F. Lorrain.. Electromagnetic Fields and Waves, *Third Edition. W.H. Freeman & Company, New York*. pp. 754, April. 1988.

[53] G. Franksenstein and R. Garner, "Equations for determining the brine volume of sea ice from− 0.5 to− 22.9° C," *Journal of Glaciology*, vol. 6, no. 48, pp. 943-944, March. 1967.

[54] D. P. Winebrenner, "Microwave sea ice signature modeling. In: Microwave Remote Sensing of Sea Ice, *Geophysical Monograph Series 68.* Washington, DC, USA: AGU, 1992.

[55] N. T. Kurtz and S. L. Farrell, "Large-scale surveys of snow depth on Arctic sea ice from Operation IceBridge," *Geophys. Res. Lett*., vol. 38, no. 20, pp. L20505, Oct. 2011.

[56] V. Alexandrov, S. Sandven, J. Wahlin and O. M. Johannessen, "The relation between sea ice thickness and freeboard in the Arctic," *The Cryosphere*., vol. 4, no. 3, pp. 373-380, Sep. 2010.

[57] R. L. Tilling, A. Ridout and A. Shepherd, "Estimating Arctic sea ice thickness and volume using CryoSat-2 radar altimeter data," *Advances in Space Research*, vol. 62, no. 6, pp. 1203-1225, Sep. 2018.

[58] R. D. C. Mallet, I. R. Lawrence, J. C. Stroeve, J. C. Landy, and M. Tsamados, "Brief Communication: Conventional assumptions involving the speed of radar waves in snow introduce systematic underestimates to sea ice thickness and seasonal growth rate estimates," The Cryosphere Discuss., *in-review*, 2019.

[59] C. Richardson, E. Aarholt, S-E. Hamran, P. Holmlund and E. Isaksson, "Spatial distribution of snow in western Dronning Maud Land, East Antarctica, mapped by a ground-based snow radar," *J. Geophys. Res.*, vol. 102, no. B9, pp. 20343-20353, Sep. 1997.

[60] R. Kwok, B. Panzer, C. Leuschen, S. Pang, T. Markus, B. Holt and S. Gogineni, "Airborne surveys of snow depth over Arctic sea ice," *J. Geophys. Res.*, vol. 116, pp. C11018, April. 2011.

[61] S. E. L. Howell, F. Laliberté, R. Kwok, C. Derksen and J. King, "Landfast ice thickness in the Canadian Arctic Archipelago from observations and models," *The Cryosphere*, vol. 10, pp. 1463-1475, July. 2016.

[62] J. King, S. Howell, C. Derksen, N. Rutter, P. Toose, J. F. Beckers, C. Haas, N. Kurtz and J. Richter-Menge, "Evaluation of Operation IceBridge quick-look snow depth estimates on sea ice," *Geophy. Resear. Lett*, vol. 42, no. 21, Nov. 2015.

[63] R. Willatt, S. W. Laxon, K. A. Giles, R. Cullen, C. Haas and V. Helm, "Ku-band radar penetration into snow cover on Arctic sea ice using airborne data," *Annals Glac*., vol. 52, no. 57, pp. 197-205, Sep. 2011.

[64] J. C. Landy, M. Tsamados and R. Scharien, "A Facet-Based Numerical Model for Simulating SAR Altimeter Echoes From Heterogeneous Sea Ice Surfaces," *IEEE Trans. Geosci. Remote Sens*., *IEEE Trans. Geosci. Remote Sens*. vol. 57, no. 7, .pp. 4164-4180. July 2019.

[65] S. G. Warren, I. G. Rigor and N. Untersteiner, "Snow Depth on Arctic Sea Ice," *Journal of Climate*, v.12, pp. 1814-1829, June. 1999.

[66] W. Moon, V. Nandan, R. K. Scharien, J. Wilkinson, J. J. Yackel, A. Barrett, I. Lawrence, R. Segal, J. Stroeve, M. Mahmud, P. J. Duke and B. Else, "Physical length Scales of Wind-Blown Snow Redistribution and Accumulation on Relatively Smooth Arctic First-Year Sea Ice," *Environmental Research Letters*, vol. 14, no.10, pp. 104003, Sep. 2019.

[67] R. C. Willatt, K. A. Giles, S. W. Laxon, L. S. Drake and A. P. Worby, "Field Investigations of Ku-Band Radar Penetration Into Snow Cover on Antarctic Sea Ice," *IEEE Trans. Geosci. Remote Sens*, vol. 48, no. 1, .pp. 365-372. Jan. 2010.

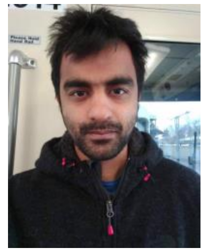

Vishnu Nandan received his Ph.D. degree in Geography from the University of Calgary, AB, Canada, where his research focused on characterizing multi-frquency microwave interactions of snow covered Arctic and Antarctic sea ice. He received his M.Sc in Earth Observation Sciences from ITC, University of Twente, The Netherlands. In 2019, he joined the Centre for Earth Observation Science (CEOS) at the University of Manitoba, Canada, as a post-doctoral research associate, where his research focuses on improving snow and sea ice thickness estimates from radar altimetry. From 2018-19, he was a post-doctoral researcher at the University of Victoria, BC, Canada, where he focused on characterizing microwave interactions from snow covered Antarctic sea ice.

Randall K. Scharien received the bachelor's degree (Hons.) from the University of Manitoba, Winnipeg, MB, Canada, in 2000, and the master's and Ph.D. degrees in microwave remote sensing of sea ice from the University of Calgary, Calgary, AB, Canada, in 2004 and 2010, respectively. From 2013 to 2014, he was a Changing Earth Science Network Investigator with European Space Agency, a position held at the Centre for Earth Observation Science, Winnipeg. In 2014, he joined the Department of Geography, University of Victoria, Victoria, BC, Canada, as a Faculty Member of remote sensing. His research interests include microwave remote sensing, synthetic aperture radar, and atmosphere–ice–ocean exchange processes.

Torsten Geldsetzer received the Ph.D. degree from the University of Calgary, Alberta, Canada, investigating the dielectric and polarimetric scattering properties of snow-covered sea ice. From 2008 to 2012, he was an Environmental Scientist with the Canada Centre for Remote Sensing, Natural Resources Canada, involved in researching and developing advanced SAR applications for cryosphere and water monitoring. Since 2012, he is a Research Associate with the Department of Geography, University of Calgary. He is concurrently an independent Consultant focusing on microwave remote sensing of snow, ice, and water; an Adjunct Assistant Professor with the Department of Geography, University of Calgary; and a Physical Scientist with the Canada Centre for Mapping and Earth Observation, Natural Resources Canada.

Ronald Kwok (Fellow IEEE) received the B.Sc.(summa cum laude) degree from Texas A&M University, College Station, TX in 1976 and the Ph.D. degree from Duke University, Durham, N.C. in 1980. He was a postdoctoral fellow at the University of British Columbia, Vancouver, BC, Canada. He is a Senior Research Scientist at the Jet Propulsion Laboratory, Pasadena CA, which he joined in 1985. His research interests include the mass and energy balance of the Arctic and Southern Ocean ice cover and the role of the sea ice in global climate, with current focus on the analysis of thickness, small-scale sea ice kinematics, and time varying gravity from various spaceborne and airborne instruments. He has over 200 referred publications and numerous articles on the state of the polar regions.

John J. Yackel received the B.A. (Hons.) degree from Wilfrid Laurier University, Waterloo, ON, Canada, in 1991, the M.Sc. degree from the University of Calgary, Calgary, AB, Canada, and the Ph.D. degree in climatology and remote sensing from the Center for Earth Observation Science, University of Manitoba, Winnipeg, MB, Canada, in 2001.

In 2000, he joined the Cryosphere Climate Research Group, Department of Geography, University of Calgary. His research interests include the role of snow in sea ice thermodynamic processes during the transition from winter through summer melt; polarimetric multifrequency microwave scatterometry, altimetry and synthetic aperture radar data for geophysical inversion of snow properties; time series microwaveoptical remote sensing for sea ice-albedo melt transitions; and detection of oil and contaminants in snow-covered sea ice from multifrequency polarimetric scatterometry using natural and mesoscale laboratory environments.

Mallik S. Mahmud received the B.Sc. degree (Hons.) in geography and environment from the University of Dhaka, Dhaka, Bangladesh, in 2011, and the M.Sc. degree in geography from the University of Calgary, Calgary, AB, Canada, in 2016, where he is currently pursuing the Ph.D. degree in microwave remote sensing. He was a Lecturer of geography and environment with the University of Dhaka. His research interests include multi-frequency microwave remote sensing of Arctic sea ice, with a focus on synthetic aperture radar imagery to monitor dynamic and thermodynamic regimes of Arctic sea ice.

Anja Rösel received the Diploma degree from Ludwig-Maximilians University in Munich, Germany in 2002 and the Ph.D. degree from the University of Hamburg, Hamburg, Germany, in 2012. Her research interests include sea ice, snow mass balance from observations, and remote sensing of sea ice. She is currently emplyoyed at the the Remote Sensing Technology Institute (IMF), German Aerospace Center (DLR), Oberpfaffenhofen, Germany, in the department EO Data Science as a research scientist. Before, she was a postdoctoral researcher at the Norwegian Polar Institute, Tromsø, Norway.

Rasmus Tonboe is at the Danish Meteorological Institute in Copenhagen. His research interests include microwave and infrared remote sensing of sea ice in particular modelling of thermal emission and backscatter from sea ice and the use of forward model inversion for estimating sea ice snow cover, and other properties.

He has field work experience, operating radiometers in the field, snow and sea ice sampling, and installing meteorological monitoring stations on sea ice. He is a member of ESA's MetOp SG MWI and ICI science advisory group and the ESA CIMR mission advisory group.

Mats Granskog received the the Ph.D. degree geophysics (hydrosphere) from the University of Helsinki, in 2004. He has worked in the Oceans and Sea Ice group at the Norwegian Polar Institute, Tromsø, Norway, since 2008, where he is a Senior Research Scientist for sea ice and polar oceanography. His research interests include sea ice geophysics, including sea ice mass and energy balance in the Arctic Ocean.

Rosemary Willatt received an MSci degree in Astronomy in 2006, and PhD in Geophysics in 2012, from University College London, UK. She is currently a Postdoctoral Research Fellow at the Centre for Polar Observation and Modelling, Earth Sciences, University College London. Her research looks at remote sensing of sea ice, particularly radar interaction with snow cover on sea ice. She has fieldwork experience in the Arctic and Antarctica, operating from ship/aeroplane.

Julienne Stroeve received her PhD in 1996 from the University of Colorado focused on documenting Greenland energy balance from satellites. Afterwards she became a senior scientist at the National Snow and Ice Data Center at CU-Boulder. Today she is a Professor at the Centre for Polar Observation and Modelling in the Earth Sciences Department at the University College London and holds a Canada 150 Chair at the University of Manitoba.

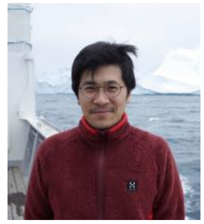

Daiki Nomura got his Ph.D. at Hokkaido University in 2008. His main research is sea ice biogeochemistry, especially for gas exchange process between sea ice and atmosphere. After Ph.D., he worked at the National Institute of Polar Research as Post-Doctoral Fellow for Antarctic sea ice biogeochemistry. Then, he moved to Norwegian Polar Institute as Post-Doctoral Fellow for Arctic research and back to Institute of Low Temperature Science, Hokkaido University in 2013. He joined N-ICE 2015 expedition for sea ice research. From October 2015, he joined the Faculty of Fisheries Sciences, Hokkaido University, Hakodate, Japan.

Markus Frey joined the British Antarctic Survey in 2008 after working for CNRS at the Laboratoire de Glaciologie et Géophysique de l'Environnement in Grenoble/France (2006-08). He received hid Ph.D. in Hydrology and Atmospheric Sciences from the University of Arizona in Tucson AZ / USA (1999-2005), and prior to that a MSci in Hydrology from the Albert-Ludwigs Universität Freiburg / Germany (1993-99). His research is about physical and chemical air-snow exchange processes to gain a better understanding of how snow and ice surfaces influence atmospheric composition and oxidation capacity, and ultimately climate, with a focus on tropospheric ozone, the nitrogen and sulfur cycle, halogen chemistry, as well as aerosol formation and growth. To date, he has lead and managed 14 atmospheric sampling and ice coring projects on expeditions to Antarctica, the Arctic and the Bolivian Andes, including two polar sea ice cruises during winter

This article has been accepted for publication in a future issue of this journal, but has not been fully edited. Content may change prior to final publication. Citation information: DOI 10.1109/JSTARS.2020.2966432, IEEE Journal of Selected Topics in Applied Earth Observations and Remote Sensing